The Impact of Submesoscale Physics on Primary Productivity of Plankton

Amala Mahadevan

Woods Hole Oceanographic Institution, Woods Hole, Massachusetts 02543;
email: amala@whoi.edu

Annu. Rev. Mar. Sci. 2016. 8:161–84

First published online as a Review in Advance on September 21, 2015

The *Annual Review of Marine Science* is online at marine.annualreviews.org

This article's doi:
10.1146/annurev-marine-010814-015912

Keywords

submesoscale, fronts, eddies, mixed layer, phytoplankton, nutrients, primary production

Abstract

Life in the ocean relies on the photosynthetic production of phytoplankton, which is influenced by the availability of light and nutrients that are modulated by a host of physical processes. Submesoscale processes are particularly relevant to phytoplankton productivity because the timescales on which they act are similar to those of phytoplankton growth. Their dynamics are associated with strong vorticity and strain rates that occur on lateral scales of 0.1–10 km. They can support vertical velocities as large as 100 m d^{-1} and play a crucial role in transporting nutrients into the sunlit ocean for phytoplankton production. In regimes with deep surface mixed layers, submesoscale instabilities can cause stratification within days, thereby increasing light exposure for phytoplankton trapped close to the surface. These instabilities help to create and maintain localized environments that favor the growth of phytoplankton, contribute to productivity, and cause enormous heterogeneity in the abundance of phytoplankton, which has implications for interactions within the ecosystem.

1. INTRODUCTION

More than half of the primary production on Earth occurs in the surface layer of the ocean and involves the photosynthetic fixation of carbon by phytoplankton (Field et al. 1998). But unlike terrestrial plants, the oceanic primary producers, phytoplankton, are subject to the vagaries of a continually moving and evolving medium. The physics of the upper ocean impacts phytoplankton growth by providing access to light and nutrients, but conditions are ripe for high growth rates only in certain places and at certain times. These sites of concentrated growth make a disproportionately large contribution to the productivity and diversity of oceanic ecosystems and to the global carbon cycle. Regions of the ocean that exhibit high rates of net primary production exhibit greater variability in the phytoplankton distribution (**Figure 1**). This review addresses some of the physics that supports phytoplankton growth, leading to hot spots of production at scales of 0.1–10 km that have significant implications for the oceanic ecosystem.

At length scales greater than a few kilometers, oceanic flow is dominated by the effects of Earth's rotation, which constrains the motion to be largely horizontal and in geostrophic and thermal wind balance. These dynamics support mesoscale instabilities and eddies of order 10–100 km that have a significant impact on the ocean's primary productivity (McGillicuddy 2016). However, recent work has revealed a host of instabilities on spatial scales of order 0.1–10 km and on timescales of a few inertial periods (∼days) that can overcome these large-scale balances (Molemaker et al. 2005) to generate vertical motion and enhanced mixing in localized regions, particularly in the surface layer of the ocean (Capet et al. 2008a–d, Haine & Marshall 1998, Klein et al. 2008, Mahadevan 2006, Mahadevan & Tandon 2006, Pollard & Regier 1990, Rudnick 1996, Shay et al. 2003). Because the typical spatial and temporal scales of these instabilities are smaller than those associated with

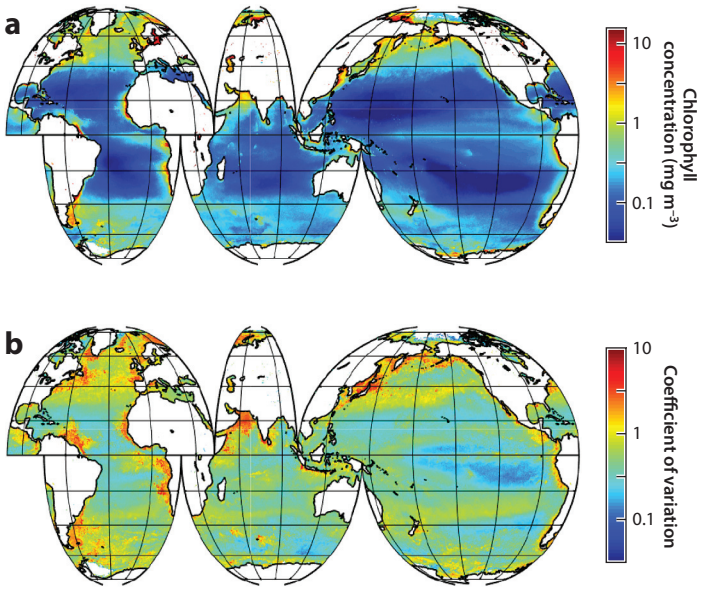

Figure 1

(*a*) Annual mean chlorophyll concentration of the oceans calculated from 9 km × 9 km level 3 binned SeaWiFS (Sea-Viewing Wide Field-of-View Sensor) data over the mission duration (1997–2010). (*b*) Coefficient of variation (standard deviation divided by mean) of sea surface chlorophyll estimated in each grid cell over the entire data record. The data have many gaps due to cloud cover. Figure courtesy of M.M. Omand.

mesoscale baroclinic instability in the pycnocline, they have come to be known as submesoscale. In this article, I use the term submesoscale in the dynamical sense, i.e., not merely as a length scale, but rather to refer to processes characterized by $O(1)$ Rossby and Richardson numbers (for a review, see Thomas et al. 2008). Although submesoscale processes are localized in space and time, they have major implications for the productivity of phytoplankton because the timescales on which they transport or change properties are similar to those of phytoplankton growth.

The factors that modulate the growth of phytoplankton are complex, depending on the species and their physiological characteristics. But broadly, and for the purposes of this discussion, light and nutrients are regarded as the primary drivers of phytoplankton primary production. Phytoplankton abundance is also affected by grazing, and although such top-down control (Behrenfeld & Boss 2014) is important, I address only the bottom-up drivers of primary production in this review.

Photosynthetically available radiation (light) decreases exponentially with depth and can support photosynthesis only in the near surface (upper 100 or so meters of the ocean). Phytoplankton nutrients (e.g., nitrate, phosphate, silicate, and iron), on the other hand, are consumed by phytoplankton in the presence of sunlight but are increasingly abundant at depth, where they are restored through the remineralization of sinking organic matter or by advection from regions where they are more abundant, such as the continental margins. Regions of the oceans that receive plenty of sunlight exhibit nutrient-depleted or oligotrophic surface conditions. The subtropical gyres are examples of such environments, where phytoplankton production is typically limited by nutrient availability. Relatively low levels of phytoplankton biomass contribute to clear waters and deeper penetration of light. These regions are marked by weak seasonality in the depth of the mixed layer. The higher latitudes (subpolar gyres), by contrast, experience a strong seasonality in mixed-layer depth. Although deep convective mixing entrains nutrients into the surface mixed layer in winter, phytoplankton growth is limited and unable to utilize all the nutrients. Low levels of sunlight and short daylight hours, coupled with transport to depths of several hundred meters by turbulent eddies in the surface mixed layer, deprive phytoplankton of the light necessary for high growth rates during winter. These regions experience enormous spring blooms when light limitation is overcome (Siegel et al. 2002).

Depending on the dynamical conditions, nutrient distributions, light environment, and growth of the phytoplankton species themselves, submesoscale physics contributes to phytoplankton production in various ways. An immense range of biophysical interactions are possible (Flierl & McGillicuddy 2002, Gargett & Marra 2002), but this article focuses only on a class of submesoscale processes. Section 2 describes some of their underlying dynamics. These dynamics appear in a physical parameter space that occurs in a range of environments, including the subtropical and subpolar gyres, the Arctic and Southern Oceans, continental shelves, and coastal seas. Rather than address these environments individually, the review lays out some general mechanisms that come into play and discusses the resulting spatial and temporal variability of the biological distributions (Section 3).

In nutrient-depleted regions, submesoscale dynamics leading to vertical motion serve to enhance the transport of nutrients from the subsurface into the euphotic layer, thereby increasing phytoplankton productivity, although in smaller areas and more episodically than is achieved through mesoscale dynamics. Section 4 describes the role of vertical transport in phytoplankton production and its dependence on the underlying distribution of the nutrients themselves.

In light-limited regions, where the upper ocean is replete with nutrients, submesoscale eddies can modulate the mixed-layer stratification and availability of light to trigger phytoplankton blooms. In such regions, submesoscale dynamics and their relationship to the surface fluxes of heat and momentum are crucial in setting the stratification. Section 5 describes the interplay of these processes.

In submesoscale phenomena, both vertical and lateral motion are intrinsically linked in terms of how the dynamics contribute to production. Although the dynamics at horizontal length scales of 0.1–10 km are anisotropic, they invoke three-dimensional instabilities that lead to a rearrangement of properties via the flux of buoyancy and tracers in both vertical and horizontal directions. Section 6 discusses the role of submesoscale downwelling in the export of phytoplankton, which in some situations can lead to the removal of viable cells from the sunlit surface layer before the nutrients are exhausted.

An important but understudied aspect of these dynamics, described in Section 7, is the resulting patchiness of phytoplankton production in space and time that is generated through submesoscale processes. This patchiness shapes oceanic ecosystems by initiating heterogeneous concentrations of food that is essential to life and leads to the aggregation of organisms that rely on it (Benoit-Bird & McManus 2012).

2. SUBMESOSCALE DYNAMICS

The dynamics of the ocean at large horizontal scales, $\sim O$(10–100 km), are strongly influenced by Earth's rotation and the small ratio of depth (D) to length (L) scales or, equivalently, the small ratio of the Coriolis parameter (f) to the buoyancy frequency (N) arising from density stratification, $\delta = D/L \sim f/N \ll 1$. This large (meso-)scale flow is characterized by a small Rossby number, $Ro = U/fL \ll 1$ (where U is the characteristic velocity), and a large Richardson number, $Ri = N/U_z \gg 1$ (where U_z is the vertical gradient of the horizontal velocity), in the density-stratified pycnocline. The flow is largely two-dimensional, and the magnitude of the vertical velocity, $W \sim Ro\,\delta U$, is several orders of magnitude smaller than the horizontal velocity; for example, for $Ro = 0.1$, $\delta = 10^{-2}$, and $U = 0.1$ m s^{-1}, the vertical velocity $W = 10^{-4}$ m s^{-1} = O(10 m d^{-1}). By contrast, turbulence that occurs at scales of order 1 m or less is three-dimensional and more or less isotropic. Submesoscale processes, which lie in the range between the large and small scales described above, occur at $O(1)$ Ro and Ri as a result of internal instabilities or surface forcing. They arise in localized regions of the surface ocean where the vertical component of the relative vorticity, $\zeta = v_x - u_y$, attains a magnitude as large as (or larger than) the planetary vorticity f, making the local $Ro = \zeta/f = O(1)$. Buoyancy forcing and wind stress at the surface contribute to enhancing (or suppressing) such dynamics.

The paradigm for mesoscale dynamics is that regions of large vorticity are distinct from those with large lateral strain rates (Okubo 1991). With submesoscale dynamics, the largest horizontal strain rates and vorticity occur in the same locations in filaments (Mahadevan & Tandon 2006). Thus, in contrast to the mesoscale picture, high vorticity and strain are coincident at submesoscales. The implication is that horizontal stretching is large in the regions where vertical velocities are enhanced, and both strain and shear play a role in shaping the phytoplankton distribution, particularly in filaments (Johnston et al. 2009).

2.1. Fronts in the Upper Ocean

Horizontal gradients in buoyancy, or fronts, are instrumental is energizing submesoscale dynamics. Fronts occur over a wide range of scales and are ubiquitous throughout the oceans, being formed by a persistent wind stress curl or by spatially nonuniform surface fluxes of heat and freshwater. The vertical and horizontal gradients in buoyancy, $b \equiv (-g/\rho_0)\rho'$, defined in terms of the density anomaly ρ' from a reference density ρ_0, are expressed as $N^2 = \partial b/\partial z$ and $M^2 = |\nabla_{\mathrm{H}} b|$, where $\nabla_{\mathrm{H}} b = (b_x, b_y)$.

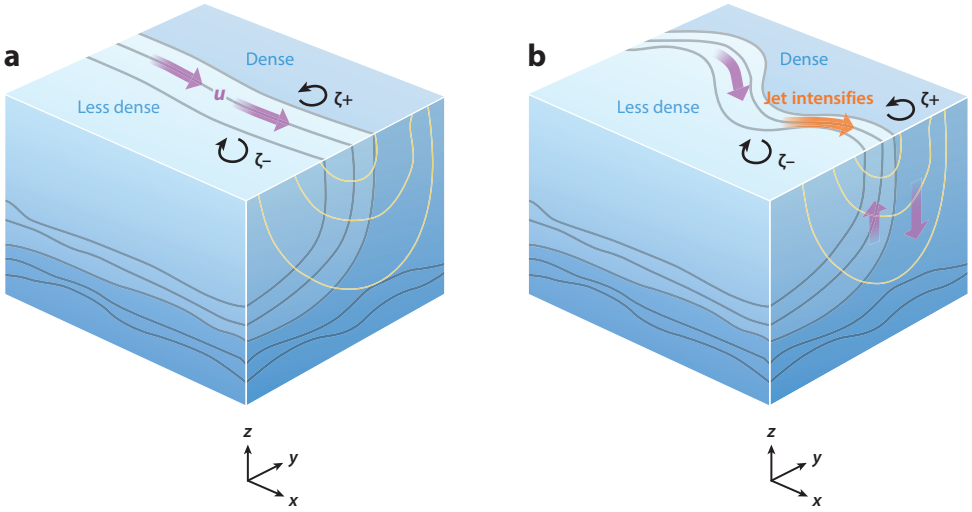

Figure 2

Schematic of an upper-ocean front, showing isopycnals (*gray lines*) separating less dense water from more dense water. The front, which is within the mixed layer, overlies a more stratified region beneath. The flow in geostrophic and thermal wind balance is along the isopycnals, as indicated by u, and its isotachs (shown in *yellow*). Such a frontal jet generates positive ($\zeta+$, cyclonic) and negative ($\zeta-$, anticyclonic) vorticity on either side. In panel *a*, the jet is more or less linear. Panel *b* shows the front after the onset of baroclinic instability, which causes it to meander and lose geostrophic balance. An ageostrophic secondary circulation with up- and downwelling is generated to restore the balance. The vertical motion becomes particularly large when the magnitude of the vorticity ζ associated with the front is of the order of the planetary vorticity f [i.e., $Ro = O(1)$] and submesoscale dynamics come into play. Depending on the depth and strength of the vertical motion and the depth of the underlying nutrient-replete layers, frontal upwelling can transport nutrients into the surface euphotic layer for phytoplankton production.

2.1.1. Frontogenesis. Even though buoyancy is conserved by the flow in the absence of buoyancy forcing (i.e., $D_t b = \partial_t b + u\partial_x b + v\partial_y b = 0$, neglecting vertical advection), the horizontal buoyancy gradient $\nabla_H b = (b_x, b_y)$ can evolve with the flow due to the presence of horizontal velocity gradients created by baroclinic instability and the meandering of the frontal jet. This evolution is expressed as

$$\nabla_H(D_t b) = D_t \nabla_H b = (-u_x b_x - v_x b_y, -u_y b_x - v_y b_y), \quad (1)$$

where $D_t = \partial_t + u\partial_x + v\partial_y$.

Frontogenetic intensification of $\nabla_H b$ is facilitated at the upper boundary of the ocean and leads to intensification of the frontal jet (along the x direction) owing to enhanced thermal wind shear, $u_z = -b_y/f$, which leads to a smaller Richardson number and an increase in the horizontal component of the vorticity. This, in turn, increases the cross-frontal (y direction) lateral shear u_y and the vertical vorticity $\zeta = v_x - u_y$ on either side of the jet (**Figure 2**). The vertical component of vorticity ζ can become as large as the planetary vorticity f in narrow regions around the front when it intensifies. Locally, the Rossby number $Ro = \zeta/f$ becomes $O(1)$, and the loss of geostrophic balance leads to an ageostrophic secondary circulation (in the plane normal to the frontal jet), which tries to restore the geostrophic and thermal wind balance at the front. The vertical velocity, which scales as $W \sim Ro\delta U$, becomes large as a result of the secondary circulation. For example, $W = 10^{-3}$ m s^{-1} $= O(100$ m d$^{-1})$ when $U = 0.1$ m s^{-1}, $\delta = 10^{-2}$, and $Ro = O(1)$.

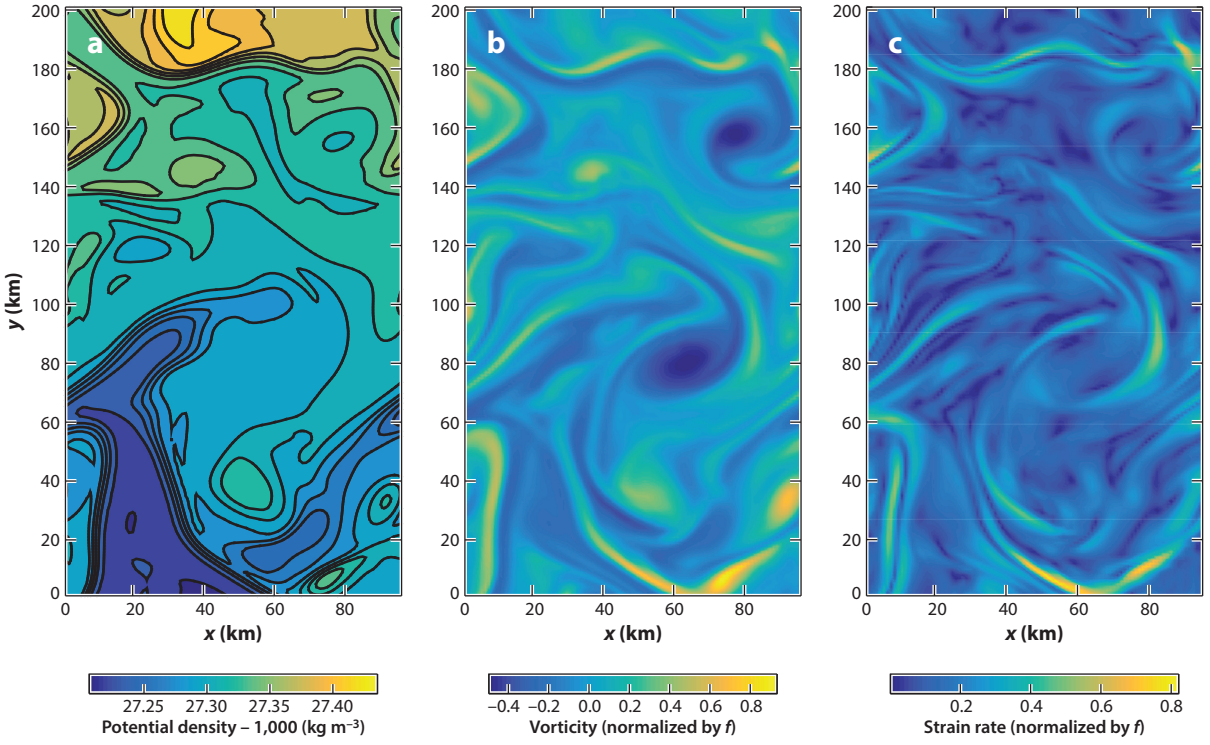

Figure 3

Model flow field at 100-m depth, showing active submesoscale dynamics. (*a*) The density displays horizontal gradients that are locally intensified. (*b*) The vertical component of the vorticity $\zeta = v_x - u_y$ normalized by the planetary vorticity f also shows regions of intensification, with positive values exceeding negative. (*c*) The strain rate $S = [(u_x - v_y)^2 + (v_x + u_y)^2]^{1/2}$ normalized by f is enhanced in the same regions where vorticity is large. The simulations were performed with the Process Study Ocean Model (Mahadevan et al. 1996a,b).

The strongest relative vorticity ζ associated with submesoscale processes appears in filaments aligned with the contours of buoyancy (**Figure 3**), and cyclonic vorticity tends to become more intense than anticyclonic vorticity (Shcherbina et al. 2013, Thomas et al. 2008), which is constrained from exceeding f in magnitude. Consequently, the vertical velocity associated with $O(1)$ Rossby-number dynamics is asymmetric, with the downwelling being more intense and occupying a smaller fraction of the area than the upwelling (Mahadevan & Tandon 2006). The horizontal strain rate $S = [(u_x - v_y)^2 + (v_x + u_y)^2]^{1/2}$ is large and of the same order of magnitude as ζ in narrow filaments where ζ is large.

2.1.2. Vertical velocity at fronts. The vertical velocity associated with the mesoscale circulation of the front can be diagnosed by the quasi-geostrophic omega equation for vertical velocity w (Allen & Smeed 1996, Rudnick 1996, Shearman et al. 1999, Tintore et al. 1991):

$$\nabla_H^2(N^2 w) + f_0^2 \frac{\partial^2 w}{\partial^2 z} = \nabla_H \cdot \mathbf{Q}, \qquad (2)$$

where the vector $\mathbf{Q} = 2(-u_x b_x - v_x b_y, -u_y b_x - v_y b_y)$ includes the frontogenetic forcing that appears in Equation 1. However, this equation fails to capture $O(1)$ Rossby-number dynamics

because the quasi-geostrophic approximation assumes $Ro \ll 1$ and neglects advection by the ageostrophic velocity. The semi-geostrophic form of the omega equation, which is more appropriate for submesoscale dynamics, is untractable on account of localized regions of negative Ertel potential vorticity (EPV) in a submesoscale flow field (Thomas et al. 2008). The negative EPV renders the Laplacian operator indefinite as the elliptic form of the equation changes to hyperbolic. An alternative approach to diagnosing vertical velocities is to use the surface quasi-geostrophic model (LaCasce & Mahadevan 2006, Lapeyre & Klein 2006, Klein & Lapeyre 2009), which is based on surface anomalies of density, but also uses the quasi-geostrophic approximation and has the limitation of not capturing submesoscale $O(1)$ Rossby-number dynamics. The recently proposed surface semi-geostrophic model (Badin 2013) overcomes some of these limitations and captures the characteristics of submesoscale flows more successfully.

2.2. Nonlinear Interactions

Observationally, submesoscale processes are difficult to distinguish from internal waves (Bühler et al. 2014) on account of their similar near-inertial timescales and the nonlinear interactions between the vorticity of the flow and the waves (Brunner-Suzuki et al. 2014, Klein et al. 2004). The strong vorticity of submesoscale dynamics is particularly effective in modifying near-inertial waves and their energy propagation (Kunze 1985), which has implications for the transfer of energy from one scale to another.

Submesoscale dynamics can also generate strong nonlinear Ekman pumping (Thomas & Rhines 2002). The vorticity at the front ζ, being $O(f)$, modulates the magnitude of Ekman transport as $M_E = \tau[\rho(f+\zeta)]^{-1}$, where τ is the wind stress. The Ekman pumping velocity, which is the vertical velocity arising from the divergence of the Ekman transport, $w_E = \nabla \cdot M_E$, is thus intensified by the positive and negative vorticity of the frontal jet (Niiler 1969). This can lead to intense up- and downwelling in the Ekman layer and contribute to the vertical velocity field of the upper ocean (Mahadevan & Tandon 2006, Mahadevan et al. 2008).

2.3. Mixed-Layer Instability

Fronts in the surface mixed layer of the ocean are susceptible to baroclinic instability (Boccaletti et al. 2007, Stone 1970), which leads to the formation of mixed-layer eddies. The eddies grow laterally as they deepen, while drawing on the available potential energy of the fronts (Badin et al. 2011). Mixed-layer eddies cause the slumping of isopycnals and lead to restratification of the mixed layer on a timescale of days. The eddies generate a net overturning (Fox-Kemper & Ferrari 2008, Fox-Kemper et al. 2008) in the vertical plane normal to the front (**Figure 4*a***), which is parameterized as a stream function (Fox-Kemper et al. 2008), $\psi_e = C_e M^2 H^2 f^{-1}$, where H is the mixed-layer depth and C_e is a scaling coefficient that lies in the range 0.06–0.08. The mean vertical and lateral buoyancy flux resulting from mixed-layer eddies scales as $\langle w'b' \rangle_e \sim \psi_e M^2$ and $\langle v'b' \rangle \sim \psi_e N^2$ (Held & Schneider 1999). The available potential energy in fronts scales with H and M^2, which explains the preponderance of submesoscale activity during winter (Mensa et al. 2013) when mixed layers are deep and fronts are not obscured by stratification.

2.4. Effects of Surface Forcing

Whereas eddies stratify the surface mixed layer, wind and convection can keep this layer well mixed. Down-front winds drive a cross-front Ekman transport of denser water to the less dense side of the front and induce convective mixing that reinforces the front (Thomas 2005, Thomas & Lee 2005).

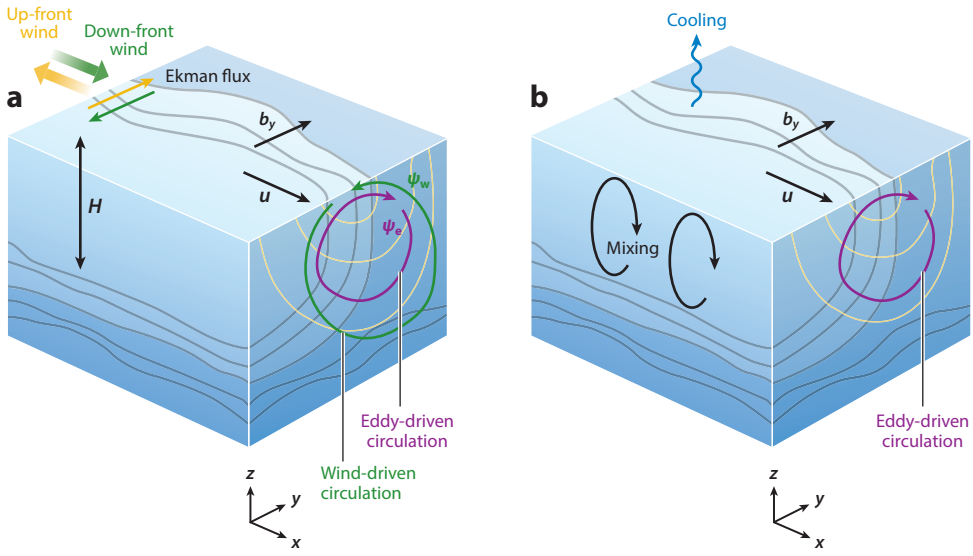

Figure 4

Schematic showing the effects of surface forcing on a front. Mixed-layer eddies generate a net overturning stream function ψ_e that tends to slump the isopycnals and restratify the mixed layer. (*a*) The down-front component of the wind stress drives an Ekman flux from the denser to the less dense side. This wind-induced overturning circulation, ψ_w (shown in *green* for down-front winds), opposes the restratifying tendency of mixed-layer eddies. Conversely, an up-front wind drives less dense water over denser water, and ψ_w (not shown for up-front winds) acts in the same direction as ψ_e, helping to restratify the mixed layer. (*b*) Surface cooling induces a vertical buoyancy flux that opposes the restratifying buoyancy flux of eddies. When the cooling is sufficiently strong, it can prevent mixed-layer eddies from stratifying the mixed layer. The along-front velocity u, the mixed-layer depth H, and the cross-front buoyancy gradient b_y are indicated in the figure.

The wind-driven overturning circulation $\psi_w = -\tau/\rho f$ counters eddy-driven overturning ψ_e when the wind is down-front (positive τ) and acts in the same direction as ψ_e when the wind has an up-front (negative τ) component (**Figure 4*a***). Thus, when $-\psi_w \geq \psi_e$, down-front winds can keep a front from restratifying. Up-front winds, on the other hand, hasten restratification (Mahadevan et al. 2010). Similarly, fronts can be maintained through a loss of heat Q from the surface of the ocean, which generates a buoyancy flux $\langle w'b' \rangle_{cool} = \alpha Qg/(\rho C_p)$, where α is the thermal expansion coefficient of the water and C_p is the specific heat capacity. When the convectively induced destratifying vertical flux of buoyancy $\langle w'b' \rangle_{cool}$ equals or exceeds the restratifying eddy-induced vertical buoyancy flux $\langle w'b' \rangle_e = C_e M^4 H^2 f^{-1}$ (**Figure 4*b***), this can prevent the mixed layer from becoming stratified (Mahadevan et al. 2012). By contrast, a positive surface buoyancy flux resulting from warming or freshwater supply will quickly stratify the mixed layer.

2.5. Symmetric Instability

The EPV, defined as $EPV = (\boldsymbol{\omega} + f\mathbf{k}) \cdot \nabla b$, is generally positive in the oceans because fN^2 is positive and dominates EPV. Here, $\boldsymbol{\omega} = \nabla \times \mathbf{u}$ is the relative vorticity vector. However, weak stratification and low Ri contribute to lowering EPV. The horizontal component of the vorticity $u_z - w_x$ contributes the term $b_y(u_z - w_x)$ to EPV, which approximates to $-u_z^2/f$ by thermal wind

balance and is a negative quantity that lowers *EPV*. (Here, x is the along-front direction, and y is the cross-front direction.) Thus, sharp fronts with a strong thermal wind shear can develop negative *EPV*, particularly in the presence of down-front winds or cooling, which tend to destratify the mixed layer. Negative *EPV* gives rise to symmetric instability, or slantwise convection (Taylor & Ferrari 2009), which restores *EPV* to a positive value by restratification over a few inertial periods. Such transient restratification can initiate phytoplankton blooms at fronts in light-limited regimes (Taylor & Ferrari 2011a).

3. SPATIAL AND TEMPORAL SCALES OF VARIABILITY

Satellite views of surface chlorophyll reveal a heterogeneous distribution of phytoplankton, continually evolving under the influence of the dynamic oceanic flow field (**Figure 5**). Analysis of the

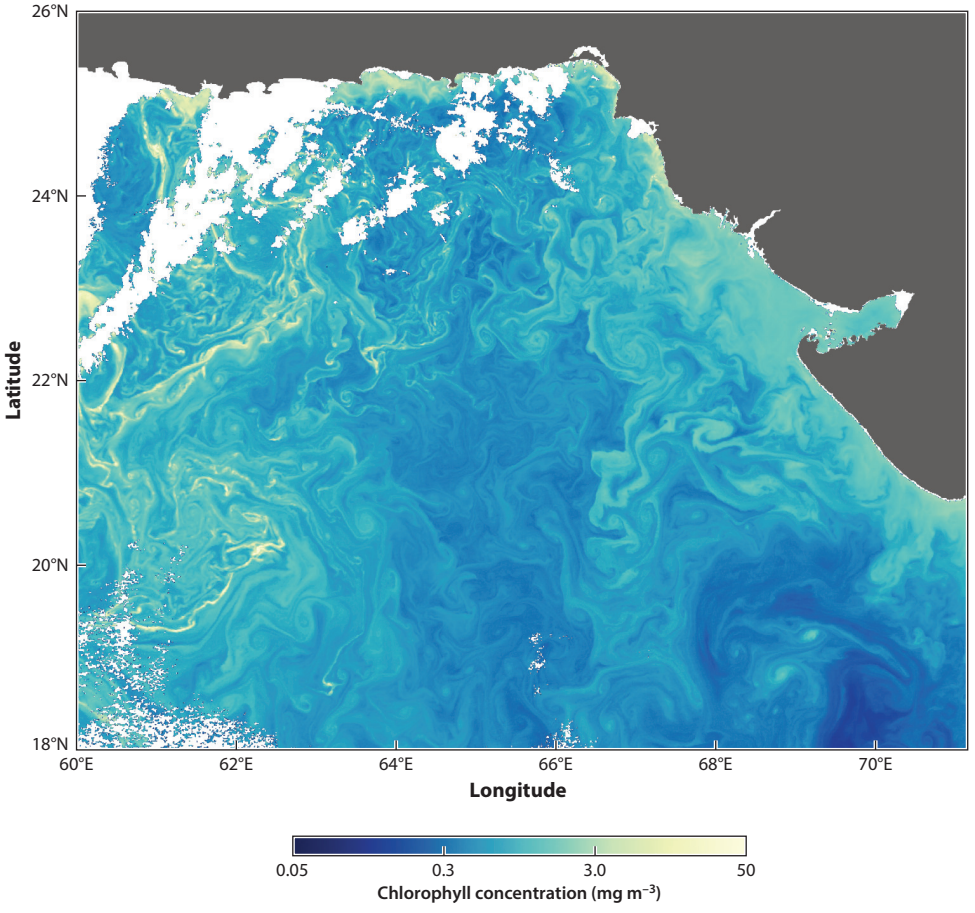

Figure 5

Sea surface chlorophyll concentration in the Arabian Sea as viewed by the Moderate Resolution Imaging Spectroradiometer (MODIS) from NASA's Aqua satellite on February 22, 2005. The chlorophyll is modulated by the ocean's dynamics and bears the signature of eddies and fronts. It displays variability over a wide range of spatial scales. The approximate resolution of the data is 1 km. White spaces are where data were flagged or missing because of cloud cover. Image courtesy of Norman Kuring, MODIS Ocean Color Team.

variance in surface chlorophyll and temperature reveals a continuous, power-law distribution of variance V over a range of length scales L, extending from the mesoscale to the kilometer scale (Callies & Ferrari 2013, Klein et al. 2011). Concurrent satellite-derived sea surface chlorophyll and temperature data at 1-km resolution from the Moderate Resolution Imaging Spectroradiometer (MODIS) reveal that chlorophyll exhibits proportionately greater variance at small scales than temperature, thereby making the $V(L)$ curve for chlorophyll flatter than that of temperature in each case examined (Mahadevan & Campbell 2002).

The horizontal stirring of a tracer with a concentration gradient generates filamentation, which leads to a downscale cascade of tracer variance (Abraham 1998). The advection of properties at the sea surface is dominated by horizontal velocities that are two to four orders of magnitude larger than vertical velocities and affect the distribution of phytoplankton, as revealed by sea surface chlorophyll (d'Ovidio et al. 2010, Lehahn et al. 2007). However, phytoplankton are also highly sensitive to vertical motion owing to the strong vertical gradient in light and nutrients. Submesoscale processes induce vertical transport at scales of order 1 km, which delivers nutrients and induces growth of phytoplankton and also moves phytoplankton vertically toward (or away from) light or nutrients. Thus, submesoscale processes inject variance at the 1-km (and possibly smaller) scale, which can be transferred upscale with time, through the translation of upwelling regions and by horizontal advection. Such a contribution of submesoscale processes to patchiness differs from that of two-dimensional stirring in that it induces high growth rates and enhanced productivity at the scale of the physics. However, the effects of horizontal and vertical advection on phytoplankton are so convolved that it is difficult to distinguish them, or the contributions of new production and horizontal stirring to the chlorophyll, in satellite data (**Figure 5**) and observations (Chavez et al. 1991).

The spatial and temporal variability of chlorophyll are related because the concentration anomalies are in the advective frame and because spatial variability appears as temporal variability when moved by the flow past a reference point. The mean and variance observed in satellite data show significant differences from one region to another (**Figure 1**). Chlorophyll is log-normally distributed (Campbell & Aarup 1992), and notably, regions with high mean values of chlorophyll are also where chlorophyll exhibits the greatest variance. These regions—the coastal zones, subpolar gyres, and Southern Ocean—are some of the most productive regions of the world's oceans, and also have a high degree of variability. The temporal variance in **Figure 1*b*** is only partly from seasonality; it contains shorter-term fluctuations in phytoplankton production and a spatial variability that translates to temporal variability through advection by the eddy field. Regions exhibiting high variance are also the regions where strong lateral density gradients and deep mixed layers enhance submesoscale activity. Process modeling studies suggest that submesoscale processes enhance not only the productivity of phytoplankton, but also its variance on shorter timescales (~days), in much the same way as mesoscale eddies enhance interannual variability (Lévy et al. 2014b) and phytoplankton diversity (Baltar et al. 2010, Hansen & Samuelsen 2009, Lévy et al. 2014a, Lima et al. 2002). Patchy productivity (Martin 2003, Martin et al. 2002, Pasquero et al. 2005) results from both vertical and lateral processes and affects the spatiotemporal distributions of plankton. Nonlinear interactions within the ecosystem are likely to be enhanced by submesoscale activity, but these may increase or suppress productivity, depending on whether the covariance of the interacting components makes a positive or negative contribution (Lévy & Martin 2013).

Although the scale-independent cascade of variance suggests that there is no scale separation at the submesoscale, it is useful to identify the horizontal length scale L_s and timescale T_s associated with the onset of baroclinic instability in the mixed layer. The length scale $L_s = NH/f = M^2H/f^2$ (where N and M refer to the vertical and lateral buoyancy gradients, respectively, in the surface

mixed layer of depth H) because in the Rossby-adjusted state, $N^2 f^2 = M^4$ (Fox-Kemper et al. 2008, Tandon & Garrett 1994). Typical values of $M^2 = 10^{-7}$ s^{-2}, $H = 100$ m, and $f^2 = 10^{-8}$ s^{-2} give a horizontal length scale $L_s = 1$ km. The corresponding timescale is $T_s = L_s/U$, where U is the advective velocity. For $Ro = O(1)$, the timescale is of the order of the inertial period $T_s = 2\pi/f$, and therefore the cumulative effects of submesoscale transport are typically evidenced within a few days.

Global patterns in primary production can be broadly characterized in terms of limitations imposed by nutrients and light (Field et al. 1998), and regimes can be identified in terms of the relative balance between the maximal light-mediated phytoplankton growth rate, the uptake of nutrients by production, and the physical processes that supply nutrients. For example, the subtropical gyres have abundant light and are nutrient limited, and because they are located far from coasts and boundaries, the uptake of nutrients by phytoplankton is balanced by its supply largely through vertical advection. The timescales of these processes—$T_V = D/W$ for vertical advection by velocity W from a depth D, and μ^{-1} for uptake by phytoplankton with growth rate μ—are approximately matched. In regions that experience deep winter mixed layers and large seasonal variations in mixed-layer depth, light limits phytoplankton growth when the mixed layer is nutrient replete. Here, the supply of nutrients is decoupled in time from phytoplankton production. These are some of the most productive regions in the world, and they experience blooms when rapid phytoplankton growth occurs in the absence of nutrient limitation over a period of a few days. In coastal upwelling regions, by contrast, offshore production may rely on the lateral transport of nutrients upwelled at the coast by eddies and filaments extending offshore (**Figure 5**). Here, the balance between supply and production implies that μ^{-1} is matched to the timescale of horizontal advection $T_H = L/U$, where U is the horizontal velocity supplying nutrients over the length scale L.

4. ENHANCEMENT OF NUTRIENT SUPPLY IN THE OLIGOTROPHIC SUBTROPICAL GYRES

Nutrients, such as dissolved nitrate and phosphate, are plentiful in the deep ocean but generally depleted at the surface, where they are consumed by phytoplankton. Both density stratification and Earth's rotation suppress vertical motion in the ocean. Stratification (or a small depth-to-length ratio) makes the motion anisotropic at scales beyond a few meters, and rotation induces a columnar coherence in the fluid that tends to make its dynamics two-dimensional at large scales ($\gtrapprox$10 km). Hence, the transport of nutrients from the stratified pycnocline into the surface mixed layer is one of the major limitations for phytoplankton production in many regions of the world's oceans. In places where surface fluxes of buoyancy and momentum support vertical mixing, nutrients can be entrained into the surface mixed layer from the pycnocline. In coastal settings, the interaction of currents, tides, and waves with the seabed and upwelling induced by the land-ocean boundary help to supply nutrients. In the subtropical gyres, however, these mechanisms do not serve to transport nutrients into the euphotic layer. Diapycnal mixing is weak, and Ekman pumping acts downward. Horizontal Ekman transport is thought to account for some of the nutrient transport from the gyre boundaries to the interior (Williams & Follows 1998). But to a large extent, the underlying dynamics of eddies and fronts sustain the vertical advective transport of nutrients from the subsurface into the euphotic layer.

4.1. Vertical Transport

The vertical velocity field comprises several types of motion acting on a range of spatial and temporal scales. Mesoscale eddies, which persist for several weeks or even months, can uplift

isopycnals with nutrients into the euphotic zone (McGillicuddy et al. 1998, McNeil et al. 1999, Siegel et al. 1999). Internal waves can similarly lift and lower nutrient-rich isopycnal layers, but this occurs on much shorter timescales than mesoscale eddies. The ageostrophic secondary circulation at fronts, which are endemic to the eddying flow field, support the vertical advection of nutrients along sloping isopycnal surfaces that outcrop in the euphotic layer (Klein & Lapeyre 2009, Lévy et al. 2001, Mahadevan & Archer 2000, Spall & Richards 2000). Divergence of the surface Ekman transport, which is enhanced at submesoscales by nonlinear effects (Thomas & Rhines 2002), generates transport into and out of the surface Ekman layer. Ascribing the vertical flux of nutrients to individual mechanisms (Mahadevan & Tandon 2006) is not easy because of the interdependencies among various processes and scales. For example, the confluence and strain field of the mesoscale eddying flow strengthens fronts, enhances the local isopycnal slope, and leads to submesoscale instabilities. Ekman transport can contribute to the intensification or spin-down of fronts, and energy can be exchanged between the eddying flow and internal wave field, particularly at submesoscale fronts (Nagai et al. 2015).

One way to identify the influence of submesoscale processes on the vertical velocity field and fluxes is to compare the solution from a numerical model in which submesoscale processes are resolved with one in which they are not. By changing the horizontal grid resolution in a three-dimensional ocean model, Mahadevan & Archer (2000) and Lévy et al. (2001) showed that nutrient fluxes to the euphotic zone increased significantly (two- to threefold) as the horizontal grid spacing decreased, initially from 40 km to 10 km (Mahadevan & Archer 2000) and then from 6 km to 2 km (Lévy et al. 2001). In these numerical experiments, the model domain encompassed a few internal Rossby radii. The nutrient field and the depth of the nutricline were maintained by the restoration of nutrients. The increase in vertical fluxes at higher grid resolutions is associated with resolving the convolutedness and the steepness of the fronts. With increasing horizontal grid resolution, the vorticity field shows higher maxima (and minima) as well as an asymmetry in the distribution of positive and negative vorticity, which leads to more intense downward (as compared with upward) velocities (Thomas et al. 2008) that attain magnitudes $O(100\ \mathrm{m\ d^{-1}})$ at horizontal grid resolutions of 1 km. A range of structures continue to emerge as model grids are refined to capture processes at the sub-kilometer scale (Gula et al. 2014, Shcherbina et al. 2013).

However, a much longer numerical integration on a much larger domain (∼2,000 km) with a coupled physical-biogeochemical model (Lévy et al. 2012) led to the surprising finding of reduced primary production in the more highly resolved model with 1/54° grid spacing. This experiment revealed the effects that grid resolution can have on modifying the large-scale thermocline structure, mixed-layer depth, and nutrients. Although vertical velocities are enhanced at higher resolution, the nutrients became depleted to greater depths in the submesoscale-resolving (∼2-km grid resolution) model, leading to reduced productivity.

4.2. Underlying Nutrients

The vertical flux of nutrients into the euphotic zone depends on the distribution of the underlying nutrient field (Garside 1985), which typically increases with depth. However, the increase of nitrate below the surface is better correlated with density than with depth in most regions of the ocean. On small spatial and temporal scales, this is explained by the vertical movement of isopycnal surfaces (Ascani et al. 2013, Johnson et al. 2010). But the correlation persists on large spatial and temporal scales (Omand & Mahadevan 2013) because eddies mix properties along isopycnals, and diapycnal mixing is weak. The depth of nutrient depletion is strongly dependent on the depth of penetration of light as well as on physical and biological processes that replenish the nutrients consumed by phytoplankton (**Figure 6*b***). The depth of light penetration is itself dependent on

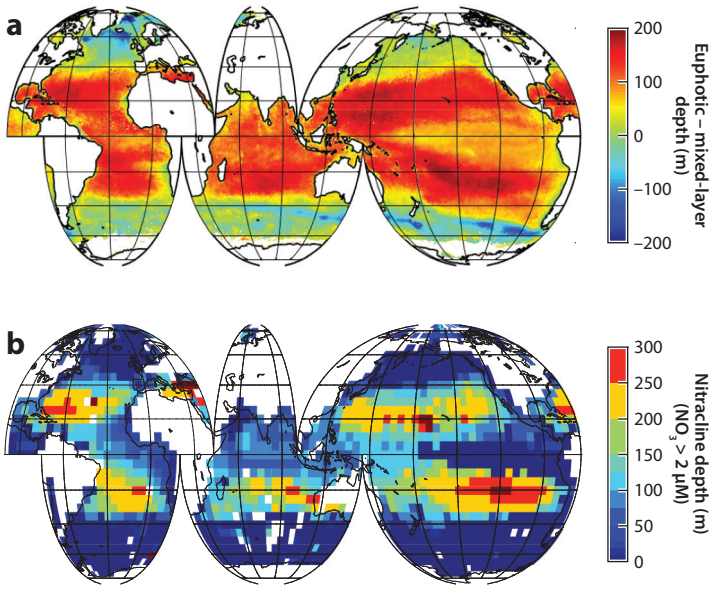

Figure 6

(*a*) Differences between the annual mean climatological euphotic layer depth and the mixed-layer depth. The euphotic depth is estimated as $z_{eu} = \log_e(0.01)K_d^{-1}$, where K_d is the attenuation coefficient obtained from level 3 binned SeaWiFS (Sea-Viewing Wide Field-of-View Sensor) data. The mixed-layer depth is from MIMOC (Monthly Isopycnal and Mixed-Layer Ocean Climatology; Schmidtko et al. 2013) and is defined as the depth at which the density differs from that of the surface bin by 0.05 kg m^{-3}. (*b*) Depths at which the nitrate concentration exceeds 2 μmol L^{-1}, estimated from the *World Ocean Atlas* 5° × 5° gridded climatology (Garcia et al. 2014). Figure courtesy of M.M. Omand.

the phytoplankton concentration, and thus there is feedback among the physical processes that supply nutrients, primary production, phytoplankton abundance, light penetration, and the depth of nutrient depletion, as well as lateral nutrient supply to the nutricline (Palter et al. 2005). In the subtropical gyres, nutrients are depleted to a greater depth than they are in subpolar regions owing to the presence of euphotic layers that are deeper than the surface mixed layer (Omand & Mahadevan 2015) throughout the year (**Figure 6*a***). Because low latitudes have less seasonality in mixed-layer depth than high latitudes, the entrainment of nutrients by deepening of the mixed layer is not as significant. Compared with the subpolar gyres, the subtropical gyres experience year-round levels of low productivity.

4.3. Vertical Extent of Upwelling

Although submesoscale processes within the mixed layer induce ageostrophic vertical velocities that can be strong, their effectiveness in supplying nutrients for primary production is dependent on the depth from which they draw water. Mixed-layer eddies typically extend the depth of the mixed layer H, and the strongest vertical velocities occur mid-depth, at $H/2$. However, many fronts extend deeper than the mixed layer (Ramachandran et al. 2014). The depth to which lateral buoyancy gradients exist in the upper ocean is crucial in determining the depth from which nutrients can be drawn. The strength of the vertical velocities depends on the available potential energy in the fronts and therefore depends on the depth and lateral buoyancy gradient of the fronts. When a strong stratification underlies the surface mixed layer and the lateral buoyancy

gradients are restricted to the mixed layer, mixed-layer submesoscale processes are not able to draw on nutrients from the pycnocline. By contrast, weaker stratification beneath the mixed layer and an extension of the lateral buoyancy gradients beneath the mixed layer lead to deeper source waters in the upwelling.

4.4. Advective Flux of Nutrients

Despite the interdependencies of processes affecting the vertical velocity field in the ocean, the vertical transport of nutrients into the euphotic zone can be separated into transport associated with the vertical movement of isopycnals and transport that occurs as an advective flux. The former includes the vertical motion by internal waves and eddy uplift. Although these mechanisms contribute to phytoplankton productivity, they are not associated with submesoscale dynamics as defined here. The advective flux, by contrast, is enhanced by submesoscale dynamics and tends to occur along isopycnal surfaces when isopycnals are upward sloping. Although the nutrient field is aligned with the isopycnal surfaces within the nutricline, there is a vertical gradient of nutrients along sloping isopycnals that outcrop into the euphotic layer. The vertical component of the (largely along-isopycnal) velocity w transports the nutrients down-gradient into the euphotic zone (**Figure 7**). The time- and space-averaged nutrient flux, denoted by c, is $\langle wc' \rangle$, where the angle brackets denote averaging in space or time and $c' = c - \langle c \rangle$ is the anomaly of the nutrient from its mean. For example, if angle brackets denote the spatial average at a fixed depth, then $\langle wc' \rangle$ is the flux in millimoles per square meter per second when w is in meters per second and c is the concentration of the nutrient in millimoles per cubic meter. The flux is thus given by the covariance between the vertical velocity w and the nutrient anomaly c' (**Figure 7**). The way in which the angle brackets, and therefore c', are defined affects the calculation of the flux.

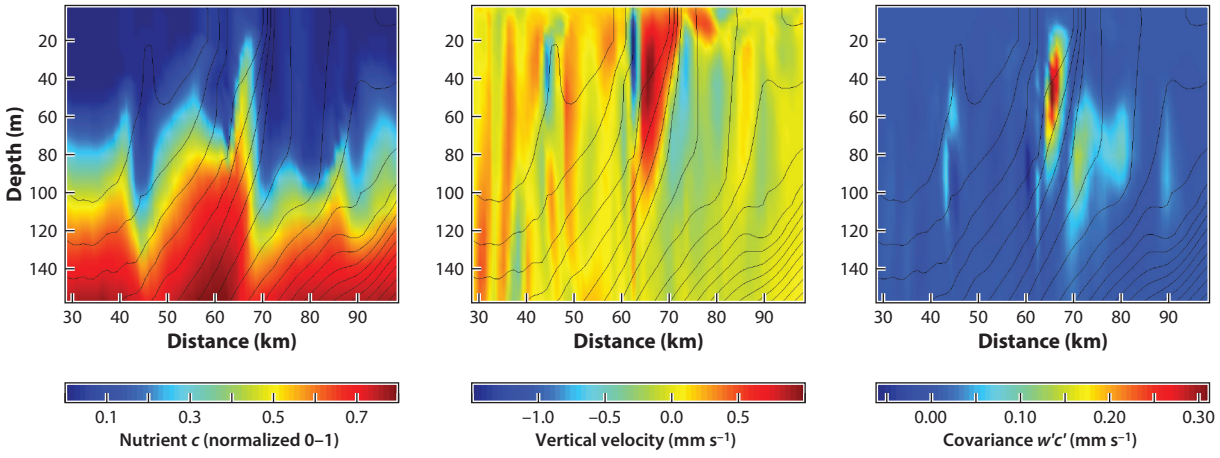

Figure 7

A vertical section from a simulation performed with the Process Study Ocean Model, showing the vertical nutrient flux in an oligotrophic setting representative of the subtropical gyres. The model uses a horizontal resolution of 1 km and a vertical resolution varying between a few meters near the surface to tens of meters at depth. The model was initialized with a typical nutrient profile throughout the domain and a horizontal density gradient that becomes unstable and generates an eddying flow field. (*a*) Nutrient c in the model is upwelled along sloping isopycnals (*black contours*) at fronts. (*b*) The vertical velocity w is enhanced at fronts. (*c*) The vertical flux of nutrients due to eddies is given by the covariance $w'c'$, where $c' = c - \langle c \rangle$, w' is the vertical velocity (which has a zero mean $\langle w \rangle = 0$), and the angle brackets denote the horizontal average. The nutrient flux is maximal where an upward (positive) velocity covaries with a positive nutrient anomaly.

Although the vertical velocity acts in both directions, the vertical nutrient gradient ensures that, on average, upward velocities transport nutrients into the euphotic layer and downward velocities transport nutrient-depleted water out of the euphotic layer. The water transported upward is not immediately returned with the downward velocities. The average secondary circulation at a front is an overturning circulation, but the upward and downward velocities do not form a closed circulation on a timescale of days. Nutrients transported upward are generally consumed by phytoplankton, and nutrient-depleted water nearer the surface is transported downward.

4.5. Coupling Between Phytoplankton Production and Physical Transport

Phytoplankton themselves affect nutrient uptake in a somewhat nonintuitive manner. Considering an area from which there are no net sources or sinks (horizontal inputs or losses) of nutrients, one can assume an approximate balance between the upward supply of nutrients into the euphotic layer and its consumption by phytoplankton. The flux of nutrients across the base of the euphotic layer is thus balanced by the phytoplankton uptake integrated over the depth of the euphotic layer given by

$$\langle wc' \rangle_{z_{eu}} = \int_{z_{eu}}^{0} \langle \mu c \rangle \mathrm{d}z, \tag{3}$$

where μ is an uptake rate for the nutrient and depends on the growth rate of the phytoplankton, the phytoplankton concentration, and the half-saturation constant. This balance shows that the vertical supply rate of nutrients $\langle wc' \rangle_{z_{eu}}$ into the euphotic layer is dependent on its rate of consumption by phytoplankton. Faster-growing phytoplankton will take up nutrients quickly, thus maintaining a nutrient-depleted euphotic layer and a stronger vertical gradient of nutrients. For the same dynamics and velocity field, the vertical flux of nutrients is greater for a phytoplankton community that is quick to consume new nutrient inputs, as compared with one that does so more slowly. This is one of the fundamental ways in which the physical delivery of nutrients is linked to the growth rates of phytoplankton. Although the notion is that nutrient supply and availability shape the phytoplankton community, the latter also affects the supply.

In a gross sense, the ecosystem adapts to optimize growth and maximize nutrient supply. Faster-growing phytoplankton, which are typically large celled, thrive and generate blooms where nutrients are more easily available. Slower-growing species of small cells are typically seen in the subtropical gyres, where the mechanisms for nutrient delivery are weaker. In a nutrient-limited setting, the uptake of nutrients is optimized when the timescales of nutrient supply into the euphotic zone are matched with those of uptake. In the framework described above, this happens when the timescale for vertical advection D/W for nutrients delivered from a depth D with typical vertical velocity W is balanced by the uptake timescale μ^{-1}. Choosing appropriate orders of magnitude—for example, $D = 100$ m and $W = 10^{-3}$ m s^{-1} $\approx$ 100 m d^{-1} for submesoscale dynamics—results in a timescale of 10^5 s or approximately a day, which is of the same order of magnitude as the growth and uptake rates of phytoplankton. This is why the more intense vertical velocities associated with submesoscale dynamics make a disproportionately large contribution to phytoplankton production.

5. EDDY-DRIVEN STRATIFICATION OF THE SURFACE MIXED LAYER IN LIGHT-LIMITED REGIMES

5.1. Seasonality of the Mixed Layer and Phytoplankton Productivity

At times and places where the surface ocean is replete with nutrients and phytoplankton growth is limited by light, an enhancement in density stratification can spur phytoplankton growth by

suppressing vertical motion in the turbulent boundary layer and enhancing exposure to light (Sverdrup 1953). Whereas air-sea fluxes of momentum and buoyancy loss from the ocean enhance turbulent mixing, submesoscale eddies generate stratification. The modulation of stratification through competing processes generates a highly variable surface boundary layer in which intense blooms of phytoplankton are initiated seasonally in the subpolar oceans through a range of mechanisms (Behrenfeld 2010, Behrenfeld & Boss 2014, Ferrari et al. 2015, Taylor & Ferrari 2011b).

In the winter, strong surface cooling and winds generate convective and wind-induced turbulence in the surface boundary layer (Brody & Lozier 2014), which deepens the mixed layer and entrains nutrients. However, the lack of light exposure caused by the low angle of sunlight, the short day length, and deep mixing, which drives phytoplankton to depths of several hundred meters, limits the growth rates of phytoplankton cells. During the spring, an increase in light exposure initiates blooms when phytoplankton take advantage of the buildup of nutrients during the winter months. However, deviations from the general pattern of seasonality described here are possible through several mechanisms (Lindemann & St. John 2014).

The oceanic mixed layer is maintained through a competition between processes that mix away the stratification and those that restore it. Fluxes of momentum, heat, and salt induced by winds, cooling, and evaporation at the air-sea interface drive shear and convective instabilities that lead to turbulent mixing and reduce stratification. Near-inertial motion can also induce shear and mixing at the base of the mixed layer. Surface fluxes of freshwater and heat, by contrast, cause stratification. Traditional mixed-layer models rely on one-dimensional budgets for density to predict the evolution of mixed-layer depth and density structure. More recently, however, studies have shown that mixed-layer eddies generated by baroclinic instability of fronts (Boccaletti et al. 2007) within the mixed layer lead to restratification of the mixed layer on a timescale of days (Fox-Kemper & Ferrari 2008, Fox-Kemper et al. 2008). This understanding has altered our thinking of how the mixed layer operates: It responds to both vertical and lateral processes, both surface fluxes and internal dynamics, and both vertical mixing and advective eddy transport.

5.2. Three-Dimensional Time Evolution of the Mixed Layer

Although the mixed layer is turbulent and well mixed during the winter, it harbors horizontal buoyancy gradients. These horizontal buoyancy gradients, or fronts, become baroclinically unstable and generate mixed-layer eddies (Boccaletti et al. 2007) with vorticity of order f along the fronts that become unstable. At the onset, the eddies have a length scale $L_s \sim M^2 H/f^2$, but they grow quickly in size as they draw energy from the available potential energy in the fronts. Mixed-layer eddies slump the fronts, converting horizontal buoyancy gradients M^2 to stratification N^2, which leads to restratification of the mixed layer on a timescale of days (Fox-Kemper & Ferrari 2008, Fox-Kemper et al. 2008). Down-front winds (the component of the wind acting in the direction of the frontal flow) cause a surface Ekman flux from the dense to the light side of the front, causing vertical mixing that counters the restratification tendency of mixed-layer eddies and keeps the front from slumping (Mahadevan et al. 2010). Similarly, surface cooling (or buoyancy loss) causes convective mixing that prevents the restratification by eddies. In winter, although mixed-layer eddies are active, the strong surface forcing prevents the mixed layer from stratifying.

In spring, as cooling and down-front winds subside, the convective deepening and mixing of the mixed layer becomes weaker. Mixed-layer eddies are then able to counter the processes that maintain the verticality of isopycnals and slump fronts. The slumping of numerous local fronts by eddies converts lateral buoyancy gradients to vertical buoyancy gradients. This submesoscale restratification is highly heterogeneous in space, generating highly variable mixed-layer depths (**Figure 8**) and, at the same time, an energetic flow field with strong vorticity and strain (as in

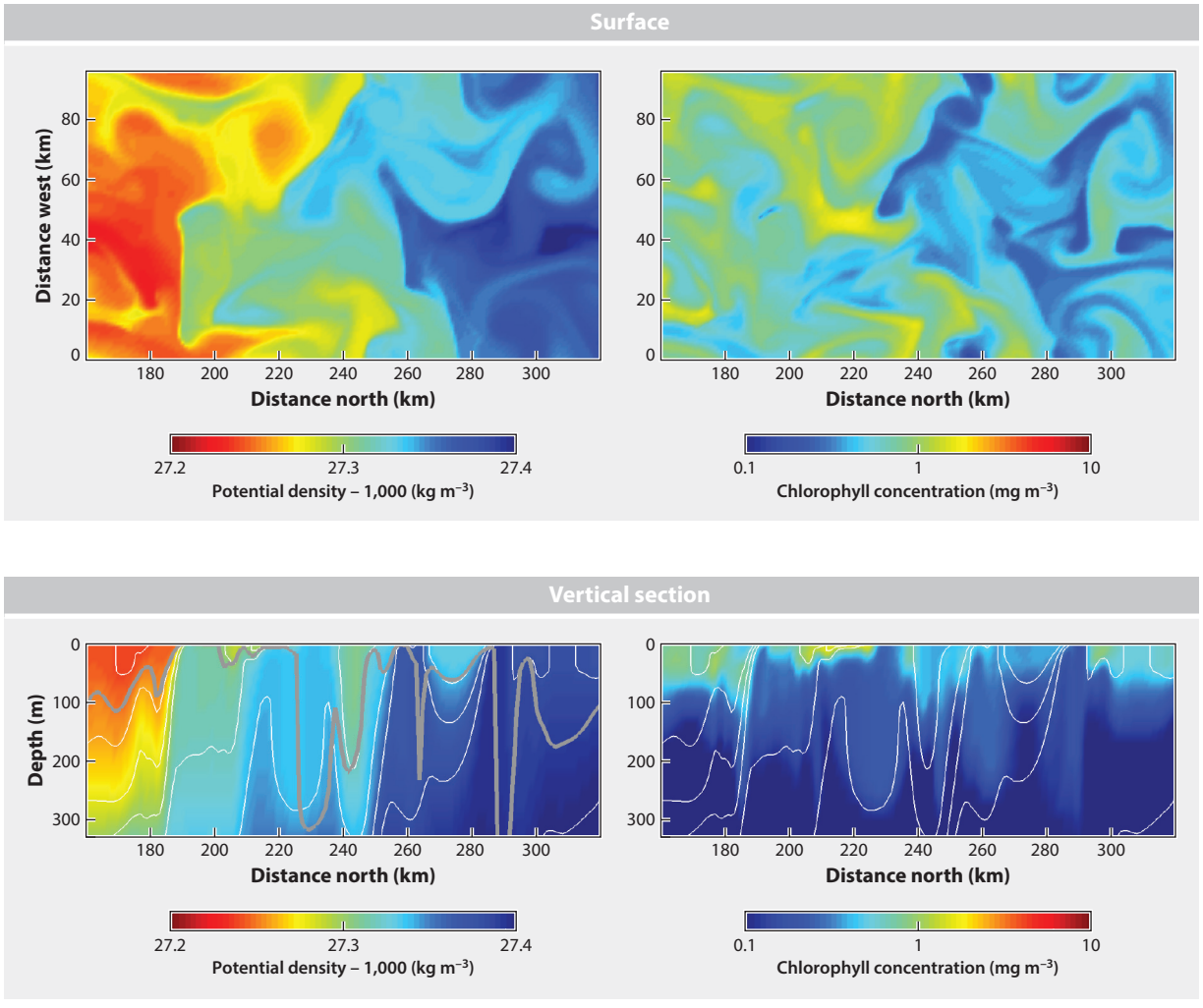

Figure 8

Mixed-layer eddies can initiate the spring phytoplankton bloom even before the onset of thermal stratification in the subpolar oceans. The top panel shows surface views of a density field that has been modified by mixed-layer eddies (*left*) and chlorophyll concentration when nutrients are abundant (*right*). The bottom panel shows the corresponding vertical sections of density (*left*) and chlorophyll (*right*). The gray line in the vertical section denotes the depth of the mixed layer using a density difference of 0.05 kg m^{-3} from the surface. White lines indicate isopycnals. The restratification generated by mixed-layer eddies is important in this light-limited regime because phytoplankton that are trapped near the surface by stratification experience more light on average and grow rapidly.

Figure 3). Phytoplankton within the mixed layer begin to see varying degrees of light. Phytoplankton trapped in near-surface stratifying regions are exposed to more light and exhibit high rates of growth, forming a bloom. Those in unstratified regions continue to be mixed to greater depths and experience less light and low growth. When mixed-layer eddies stratify the mixed layer before the onset of warming by the heat flux, the phytoplankton bloom is very inhomogeneous or patchy (Mahadevan et al. 2012). This type of bloom differs from one that is induced by thermal stratification. Eddy-induced restratification is very inhomogeneous as compared with thermally

induced stratification, and consequently the phytoplankton bloom is patchy, initiating along the edges of eddies, where stratification first sets in. The stratifying regions appear as filaments that also experience high lateral strain, causing them to be stretched and stirred such that the phytoplankton's chlorophyll distribution in satellite imagery appears to be strongly modulated by eddies.

This understanding of submesoscale eddies in the mixed layer has altered our thinking on how the structure of the mixed layer evolves. The mixed layer responds not only to surface fluxes, but also to the internal dynamics of its eddies. One of the most significant implications of mixed-layer eddies is for the productivity of phytoplankton in the upper ocean: These eddies modulate the light and nutrient environment experienced by phytoplankton within the mixed layer, thereby influencing their productivity and distributions.

6. SUBDUCTION OF PHYTOPLANKTON AND NUTRIENTS

The vertical velocities associated with submesoscale dynamics can also downwell phytoplankton, removing them from the euphotic layer. Gruber et al. (2011) found that productivity in the region of the California Current, which is infused with nutrients by coastal upwelling, is suppressed in model simulations that resolve the submesoscale dynamics of the coastal fronts. This is because phytoplankton growing from the upwelled nutrients are subducted out of the euphotic zone by the strong downward velocities before the nutrients are entirely consumed. The downward velocities are particularly intensified in cold filaments that emanate from the upwelling front. A filament consists of two fronts coming together, and the downwelling on the cold side of both fronts is compounded within the filament (Gula et al. 2014, McWilliams et al. 2009). Cold filaments are therefore effective in subducting surface water that is rich in phytoplankton.

The subduction of surface water rich in phytoplankton carbon also occurs within an eddying flow field generated by the instability of a front (Fielding et al. 2001; Guidi et al. 2012; Pollard & Regier 1990, 1992; Spall 1995). Eddy-driven subduction is effective in exporting phytoplankton from the spring bloom in the subpolar North Atlantic (Omand et al. 2015). The subduction occurs along isopycnals, with surface waters on denser isopycnals sliding beneath lighter waters on adjacent isopycnals as the mixed layer stratifies. The vertical motion is strongly linked to the vorticity of the eddying flow field, and subducting filaments are entwined in the eddies' vorticity. The downwelling of chlorophyll is also seen in observations of stronger fronts such as the Alboran front (Ruiz et al. 2009). Such submesoscale subduction exports viable phytoplankton cells from the euphotic layer and contributes to the export of carbon and oxygen from the surface ocean. However, the role of subduction in primary production cannot be considered without the processes that generate and sustain the conditions for production (Spall & Richards 2000).

7. PATCHINESS

One of the important effects of submesoscale processes is the high degree of spatiotemporal heterogeneity that they generate in phytoplankton productivity. The conditions for submesoscale dynamics emerge locally in the evolving flow field, where they may enhance nutrient supply or light exposure experienced by phytoplankton. Submesoscale processes enhance the variability in the depth of the mixed layer, and the mixed-layer buoyancy and stratification are advected with the flow to resemble the filamentous distribution of the strain and vorticity. The complex dynamics of the surface mixed layer, the variability of light and nutrients, the nonlinear response of phytoplankton growth, and the advection of phytoplankton by the flow lead to highly heterogeneous production and distributions of phytoplankton (Cunningham et al. 2003; d'Ovidio et al. 2010; Franks 1992,

1997; Lévy et al. 2014a; Lovejoy et al. 2001; Mackas 1984). Thus, irregularities in the physical conditions stemming from dynamical imbalances lead to patchy environmental conditions that at some places and times favor phytoplankton production. Such heterogeneity is fundamental to the structuring, phenology, and diversity of oceanic ecosystems (Mackas et al. 1985, Taniguchi et al. 2014). Zooplankton rely on concentrations of phytoplankton biomass, and aggregations of zooplankton (Boucher et al. 1987, Owen 1989) provide food to higher trophic levels to sustain populations of fish, mammals, and birds and maintain biodiversity. Much remains to be done in understanding the interconnectedness between submesoscale processes, primary production, and the structuring of oceanic ecosystems.

8. CONCLUDING REMARKS

Although computational modeling, satellite observations, and ship-based and autonomous measurements have greatly increased our understanding of oceanic submesoscale dynamics, it remains unclear how these processes affect the global state of the ocean. The primary production of phytoplankton is one area in which the effects of submesoscale processes are most evident. Submesoscale dynamics contribute to phytoplankton production by enhancing the supply of nutrients in regions that are nutrient limited and by generating density stratification in the surface layer to increase light exposure for phytoplankton that are light limited. These effects occur locally at scales of 0.1–10 km and over a few days and result in the heterogeneous supply and distribution of nutrients, stratification, and mixed-layer depth, which generate patches of high productivity that are thought to contribute substantially to oceanic ecosystems, their structure and phenology, and the ensuing trophic cascades.

The vertical and horizontal dynamics of submesoscale processes are intrinsically linked. Thus, the vertical supply of nutrients and downwelling of phytoplankton are closely related to the horizontal shear and vorticity of the flow, as well as the stretching of filaments through horizontal advection. The enhanced productivity of phytoplankton is manifest in filaments that are strongly affected by both the horizontal and vertical motion.

Although mesoscale turbulence contains more energy than submesoscale turbulence, submesoscale dynamics are associated with a loss of geostrophic and thermal wind balance. Submesoscale motion tends to be less constrained by Earth's rotation than mesoscale motion, and it allows for more ageostrophic circulation with greater vertical motion. Importantly, the timescale for the vertical transport of nutrients and restratification by submesoscale dynamics is similar to the timescales of phytoplankton growth and production, making these mechanisms very effective in supporting primary production. These effects are not included in current global carbon cycle models and beg the question of whether their representation is important for the structuring of the ecosystem, uptake of atmospheric CO_2, and large-scale distributions of properties in the ocean.

DISCLOSURE STATEMENT

The author is not aware of any affiliations, memberships, funding, or financial holdings that might be perceived as affecting the objectivity of this review.

ACKNOWLEDGMENTS

I am thankful for support from the National Science Foundation (NSF), the National Aeronautics and Space Administration (NASA), and the Office of Naval Research (ONR) over the years. Research on submesoscale dynamics has benefited, in particular, from two ONR Departmental

Research Initiatives: LATMIX and ASIRI. Studies of submesoscale physical-biological interactions were supported by NSF grants OCE-I434788 and OCE-0928617. I additionally benefited from a fellowship at the Radcliffe Institute for Advanced Study in 2014–2015.

LITERATURE CITED

Abraham ER. 1998. The generation of plankton patchiness by turbulent stirring. *Nature* 391:577–80

Allen JT, Smeed DA. 1996. Potential vorticity and vertical velocity at the Iceland Færoes front. *J. Phys. Oceanogr.* 26:2611–34

Ascani F, Richards KJ, Firing E, Grant S, Johnson KS, et al. 2013. Physical and biological controls of nitrate concentrations in the upper subtropical North Pacific Ocean. *Deep-Sea Res. II* 93:119–34

Badin G. 2013. Surface semi-geostrophic dynamics in the ocean. *Geophys. Astrophys. Fluid Dyn.* 107:526–40

Badin G, Tandon A, Mahadevan A. 2011. Lateral mixing in the pycnocline by baroclinic mixed layer eddies. *J. Phys. Oceanogr.* 41:2080–100

Baltar F, Arístegui J, Gasol JM, Lekunberri I, Herndl GJ. 2010. Mesoscale eddies: hotspots of prokaryotic activity and differential community structure in the ocean. *ISME J.* 4:975–88

Behrenfeld MJ. 2010. Abandoning Sverdrup's critical depth hypothesis on phytoplankton blooms. *Ecology* 91:977–89

Behrenfeld MJ, Boss E. 2014. Resurrecting the ecological underpinnings of ocean plankton blooms. *Annu. Rev. Mar. Sci.* 6:167–94

Benoit-Bird KJ, McManus MA. 2012. Bottom-up regulation of a pelagic community through spatial aggregations. *Biol. Lett.* 8:813–16

Boccaletti G, Ferrari R, Fox-Kemper B. 2007. Mixed layer instabilities and restratification. *J. Phys. Oceanogr.* 37:2228–50

Boucher J, Ibanez F, Prieur L. 1987. Daily and seasonal variations in the spatial distribution of zooplankton populations in relation to the physical structure in the Ligurian Sea Front. *J. Mar. Res.* 45:133–73

Brody SR, Lozier MS. 2014. Changes in dominant mixing length scales drive subpolar phytoplankton blooms in the North Atlantic. *Geophys. Res. Lett.* 41:3197–203

Brunner-Suzuki AMEG, Sundermeyer MA, Lelong MP. 2014. Upscale energy transfer by the vortical mode and internal waves. *J. Phys. Oceanogr.* 44:2446–69

Bühler O, Callies J, Ferrari R. 2014. Wave-vortex decomposition of one-dimensional ship track data. *J. Fluid Mech.* 756:1007–26

Callies J, Ferrari R. 2013. Interpreting energy and tracer spectra of upper-ocean turbulence in the submesoscale range (1–200 km). *J. Phys. Oceanogr.* 43:2456–74

Campbell J, Aarup T. 1992. New production in the North Atlantic derived from seasonal patterns of surface chlorophyll. *Deep-Sea Res.* 39:1669–94

Capet X, Campos EJ, Paiva AM. 2008a. Submesoscale activity over the Argentinian shelf. *Geophys. Res. Lett.* 35:L15605

Capet X, McWilliams JC, Molemaker MJ, Shchepetkin AF. 2008b. Mesoscale to submesoscale transition in the California Current system: energy balance and flux. *J. Phys. Oceanogr.* 38:2256–69

Capet X, McWilliams JC, Molemaker MJ, Shchepetkin AF. 2008c. Mesoscale to submesoscale transition in the California Current system: flow structure, eddy flux, and observational tests. *J. Phys. Oceanogr.* 38:29–43

Capet X, McWilliams JC, Molemaker MJ, Shchepetkin AF. 2008d. Mesoscale to submesoscale transition in the California Current system: frontal processes. *J. Phys. Oceanogr.* 38:44–64

Chavez FP, Barber RT, Kosro PM, Huyer A, Ramp SR, et al. 1991. Horizontal transport and the distribution of nutrients in the Coastal Transition Zone off northern California: effects on primary production, phytoplankton biomass and species composition. *J. Geophys. Res. Oceans* 96:14833–48

Cunningham A, McKee D, Craig S, Tarran G, Widdicombe V. 2003. Fine-scale variability in phytoplankton community structure and inherent optical properties measured from an autonomous underwater vehicle. *J. Mar. Syst.* 43:51–59

d'Ovidio F, Monte SD, Alvain S, Dandonneaub Y, Lévy M. 2010. Fluid dynamical niches of phytoplankton types. *PNAS* 107:18366–70

Ferrari R, Merrifield ST, Taylor JR. 2015. Shutdown of convection triggers increase of surface chlorophyll. *J. Mar. Syst.* 147:116–22
Field CB, Behrenfeld MJ, Randerson JT, Falkowski P. 1998. Primary production of the biosphere: integrating terrestrial and oceanic components. *Science* 281:237–40
Fielding S, Crisp N, Allen J, Hartman M, Rabe B, Roe H. 2001. Mesoscale subduction at the Almeria-Oran front: part 2. Biophysical interactions. *J. Mar. Syst.* 30:287–304
Flierl G, McGillicuddy DJ Jr. 2002. Mesoscale and submesoscale physical-biological interactions. In *The Sea*, Vol. 12: *Biological-Physical Interactions in the Sea*, ed. AR Robinson, JJ McCarthy, BJ Rothschild, pp. 113–85. New York: Wiley & Sons
Fox-Kemper B, Ferrari R. 2008. Parameterization of mixed layer eddies. Part II: prognosis and impact. *J. Phys. Oceanogr.* 38:1166–79
Fox-Kemper B, Ferrari R, Hallberg R. 2008. Parameterization of mixed layer eddies. Part I: theory and diagnosis. *J. Phys. Oceanogr.* 38:1145–65
Franks PJS. 1992. Phytoplankton blooms at fronts: patterns, scales and physical forcing mechanisms. *Rev. Aquat. Sci.* 6:121–37
Franks PJS. 1997. Spatial patterns in dense algal blooms. *Limnol. Oceanogr.* 42:1297–305
Garcia HE, Locarnini RA, Boyer TP, Antonov JI, Baranova OK, et al. 2014. *World Ocean Atlas 2013*, Vol. 4: *Dissolved Inorganic Nutrients (Phosphate, Nitrate, Silicate)*. Ed. S Levitus, tech. ed. A Mishonov. NOAA Atlas NESDIS 76. Silver Spring, MD: Natl. Cent. Environ. Inf.
Gargett A, Marra J. 2002. Effects of upper ocean physical processes (turbulence, advection, and air–sea interaction) on oceanic primary production. In *The Sea*, Vol. 12: *Biological-Physical Interactions in the Sea*, ed. AR Robinson, JJ McCarthy, BJ Rothschild, pp. 19–49. New York: Wiley & Sons
Garside C. 1985. The vertical distribution of nitrate in open ocean surface water. *Deep-Sea Res.* 32:723–32
Gruber N, Lachkar Z, Frenzel H, Marchesiello P, Mnnich M, et al. 2011. Eddy-induced reduction of biological production in eastern boundary upwelling systems. *Nat. Geosci.* 4:787–92
Guidi L, Calil PHR, Duhamel S, Björkman KM, Doney SC, et al. 2012. Does eddy-eddy interaction control surface phytoplankton distribution and carbon export in the North Pacific Subtropical Gyre? *J. Geophys. Res.* 117:G02024
Gula J, Molemaker MJ, McWilliams JC. 2014. Submesoscale cold filaments in the Gulf Stream. *J. Phys. Oceanogr.* 44:2617–43
Haine TWN, Marshall JC. 1998. Gravitational, symmetric, and baroclinic instability of the ocean mixed layer. *J. Phys. Oceanogr.* 28:634–58
Hansen C, Samuelsen A. 2009. Influence of horizontal model grid resolution on the simulated primary production in an embedded primary production model in the Norwegian Sea. *J. Mar. Syst.* 75:236–44
Held IM, Schneider T. 1999. The surface branch of the zonally averaged mass transport circulation in the troposphere. *J. Atmos. Sci.* 56:1688–97
Johnson KS, Riser SC, Karl DM. 2010. Nitrate supply from deep to near-surface waters of the North Pacific subtropical gyre. *Nature* 465:1062–65
Johnston T, Cheriton O, Pennington JT, Chavez FP. 2009. Thin phytoplankton layer formation at eddies, filaments, and fronts in a coastal upwelling zone. *Deep-Sea Res. II* 56:246–59
Klein P, Hua BL, Lapeyre G, Capet X, Gentil SL, Sasaki H. 2008. Upper ocean turbulence from high-resolution 3-D resolution simulations. *J. Phys. Oceanogr.* 38:1748–63
Klein P, Lapeyre G. 2009. The oceanic vertical pump induced by mesoscale and submesoscale turbulence. *Annu. Rev. Mar. Sci.* 1:351–75
Klein P, Lapeyre G, Roullet G, Le Gentil S, Sasaki H. 2011. Ocean turbulence at meso and submesoscales: connection between surface and interior dynamics. *Geophys. Astrophys. Fluid Dyn.* 105:421–37
Klein P, Smith SL, Lapeyre G. 2004. Organization of near-inertial energy by an eddy field. *Q. J. R. Meteorol. Soc.* 130:1153–66
Kunze E. 1985. Near-inertial wave propagation in geostrophic shear. *J. Phys. Oceanogr.* 15:544–65
LaCasce J, Mahadevan A. 2006. Estimating subsurface horizontal and vertical velocities from sea-surface temperature. *J. Mar. Res.* 64:695–721
Lapeyre G, Klein P. 2006. Dynamics of the upper oceanic layers in terms of surface quasigeostrophy theory. *J. Phys. Oceanogr.* 36:165–76

Lehahn Y, d'Ovidio F, Ley M, Heifetz E. 2007. Stirring of the northeast Atlantic spring bloom: a Lagrangian analysis based on multi-satellite data. *J. Geophys. Res. Oceans* 112:C08005
Lévy M, Iovino D, Resplandy L, Klein P, Madec G, et al. 2012. Large-scale impacts of submesoscale dynamics on phytoplankton: local and remote effects. *Ocean Model.* 43–44:77–93
Lévy M, Jahn O, Dutkiewicz S, Follows MJ. 2014a. Phytoplankton diversity and community structure affected by oceanic dispersal and mesoscale turbulence. *Limnol. Oceanogr. Fluids Environ.* 4:67–84
Lévy M, Klein P, Treguier AM. 2001. Impacts of sub-mesoscale physics on production and subduction of phytoplankton in an oligotrophic regime. *J. Mar. Res.* 59:535–65
Lévy M, Martin A. 2013. The influence of mesoscale and submesoscale heterogeneity on ocean biogeochemical reactions. *Glob. Biogeochem. Cycles* 27:1139–50
Lévy M, Resplandy R, Lengaigne M. 2014b. Oceanic mesoscale turbulence drives large biogeochemical interannual variability at mid and high latitudes. *Geophys. Res. Lett.* 41:2467–74
Lima ID, Olson DB, Doney SC. 2002. Biological response to frontal dynamics and mesoscale variability in oligotrophic environments: biological production and community structure. *J. Geophys. Res. Oceans* 107:25-1–21
Lindemann C, St. John MA. 2014. A seasonal diary of phytoplankton in the North Atlantic. *Front. Mar. Sci.* 1:37
Lovejoy S, Currie WJS, Claeroboudt TY, Bourget E, Roff JC, Schertzer D. 2001. Universal multifractals and ocean patchiness: phytoplankton, physical fields and coastal heterogeneity. *J. Plankton Res.* 23:117–41
Mackas DL. 1984. Spatial autocorrelation of plankton community composition in a continental shelf ecosystem. *Limnol. Oceanogr.* 29:451–57
Mackas DL, Denman KL, Abbott MR. 1985. Plankton patchiness: biology in the physical vernacular. *Bull. Mar. Sci.* 37:652–74
Mahadevan A. 2006. Modeling vertical motion at ocean fronts: Are nonhydrostatic effects relevant at submesoscales? *Ocean Model.* 14:222–40
Mahadevan A, Archer D. 2000. Modeling the impact of fronts and mesoscale circulation on the nutrient supply and biogeochemistry of the upper ocean. *J. Geophys. Res. Oceans* 105:1209–25
Mahadevan A, Campbell J. 2002. Biogeochemical patchiness at the sea surface. *Geophys. Res. Lett.* 29:1926
Mahadevan A, D'Asaro E, Lee C, Perry MJ. 2012. Eddy-driven stratification initiates North Atlantic Spring phytoplankton blooms. *Science* 337:54–58
Mahadevan A, Oliger J, Street R. 1996a. A nonhydrostatic mesoscale ocean model. Part I: well-posedness and scaling. *J. Phys. Oceanogr.* 26:1868–80
Mahadevan A, Oliger J, Street R. 1996b. A nonhydrostatic mesoscale ocean model. Part II: numerical implementation. *J. Phys. Oceanogr.* 26:1881–900
Mahadevan A, Tandon A. 2006. An analysis of mechanisms for submesoscale vertical motion at ocean fronts. *Ocean Model.* 14:241–56
Mahadevan A, Tandon A, Ferrari R. 2010. Rapid changes in the mixed layer stratification driven by submesoscale instabilities and winds. *J. Geophys. Res. Oceans* 115:C03017
Mahadevan A, Thomas LN, Tandon A. 2008. Comment on "Eddy/wind interactions stimulate extraordinary mid-ocean plankton blooms." *Science* 320:448
Martin A. 2003. Plankton patchiness: the role of lateral stirring and mixing. *Prog. Oceanogr.* 57:125–74
Martin A, Richards K, Bracco A, Provenzale A. 2002. Patchy productivity in the open ocean. *Glob. Biogeochem. Cycles* 16:9-1–9
McGillicuddy DJ Jr. 2016. Mechanisms of physical-biological-biogeochemical interaction at the oceanic mesoscale. *Annu. Rev. Mar. Sci.* 8:125–59
McGillicuddy DJ Jr., Robinson AR, Siegel DA, Jannasch HW, Johnson R, et al. 1998. Influence of mesoscale eddies on new production in the Sargasso Sea. *Nature* 394:263–66
McNeil JD, Jannasch HW, Dickey T, McGillicuddy DJ Jr., Brzezinski M, Sakamoto CM. 1999. New chemical, bio-optical and physical observations of upper ocean response to the passage of a mesoscale eddy off Bermuda. *J. Geophys. Res. Oceans* 104:15537–48
McWilliams JC, Colas F, Molemaker M. 2009. Cold filamentary intensification and oceanic surface convergence lines. *Geophys. Res. Lett.* 36:L18602

Mensa JA, Garraffo Z, Griffa A, Özgökmen TM, Haza A, Veneziani M. 2013. Seasonality of the submesoscale dynamics in the gulf stream region. *Ocean Dyn.* 63:923–41

Molemaker M, McWilliams JC, Yavneh I. 2005. Baroclinic instability and loss of balance. *J. Phys. Oceanogr.* 35:1505–17

Nagai T, Tandon A, Kunze E, Mahadevan A. 2015. Spontaneous generation of near-inertial waves by the Kuroshio Front. *J. Phys. Oceanogr.* 45:2381–406

Niiler P. 1969. On the Ekman divergence in an oceanic jet. *J. Geophys. Res.* 74:7048–52

Okubo A. 1991. Horizontal dispersion of floatable particles in the vicinity of velocity singularity such as convergences. *Deep-Sea Res.* 17:445–54

Omand MM, D'Asaro EA, Lee CM, Perry M-J, Briggs N, et al. 2015. Eddy-driven subduction exports particulate organic carbon from the spring bloom. *Science* 348:54–58

Omand MM, Mahadevan A. 2013. Large-scale alignment of oceanic nitrate and density. *J. Geophys. Res. Oceans* 118:5322–32

Omand MM, Mahadevan A. 2015. Shape of the oceanic nitracline. *Biogeosciences* 12:3273–87

Owen RW. 1989. Microscale and finescale variations of small plankton in coastal and pelagic environments. *J. Mar. Res.* 47:197–240

Palter JB, Lozier SM, Barber RT. 2005. The effect of advection on the nutrient reservoir in the North Atlantic subtropical gyre. *Nature* 437:687–92

Pasquero C, Bracco A, Provenzale A. 2005. Impact of spatiotemporal variability of the nutrient flux on primary productivity in the ocean. *J. Geophys. Res. Oceans* 110:C07005

Pollard RT, Regier L. 1990. Large variations in potential vorticity at small spatial scales in the upper ocean. *Nature* 348:227–29

Pollard RT, Regier L. 1992. Vorticity and vertical circulation at an ocean front. *J. Phys. Oceanogr.* 22:609–25

Ramachandran S, Tandon A, Mahadevan A. 2014. Enhancement in vertical fluxes at a front by mesoscale-submesoscale coupling. *J. Geophys. Res. Oceans* 119:8495–511

Rudnick DL. 1996. Intensive surveys of the Azores front: 2. Inferring the geostrophic and vertical velocity fields. *J. Geophys. Res. Oceans* 101:16291–303

Ruiz S, Pascual A, Garau B, Pujol I, Tintore J. 2009. Vertical motion in the upper ocean from glider and altimetry data. *Geophys. Res. Lett.* 36:L14607

Schmidtko S, Johnson GC, Lyman J. 2013. MIMOC: a global monthly isopycnal upper-ocean climatology with mixed layers. *J. Geophys. Res. Oceans* 118:1658–72

Shay LK, Cook TM, An PE. 2003. Submesoscale coastal ocean flows detected by very high frequency radar and autonomous underwater vehicles. *J. Atmos. Ocean. Technol.* 20:1583–99

Shcherbina AY, D'Asaro EA, Lee CM, Klymak JM, Molemaker MJ, McWilliams JC. 2013. Statistics of vertical vorticity, divergence, and strain in a developed submesoscale turbulence field. *Geophys. Res. Lett.* 40:4706–11

Shearman RK, Barth JM, Kosro PM. 1999. Diagnosis of three-dimensional circulation associated with mesoscale motion in the California current. *J. Phys. Oceanogr.* 29:651–70

Siegel DA, Doney SC, Yoder JA. 2002. The North Atlantic spring phytoplankton bloom and Sverdrup's critical depth hypothesis. *Science* 296:730–33

Siegel DA, McGillicuddy DJ Jr., Fields E. 1999. Mesoscale eddies, satellite altimetry, and new production in the Sargasso Sea. *J. Geophys. Res. Oceans* 104:13359–79

Spall MA. 1995. Frontogenesis, subduction, and cross-front exchange at upper ocean fronts. *J. Geophys. Res. Oceans* 100:2543–57

Spall SA, Richards KJ. 2000. A numerical model of mesoscale frontal instabilities and plankton dynamics—I. Model formulation and initial experiments. *Deep-Sea Res. I* 47:1261–301

Stone PH. 1970. On non-geostrophic baroclinic stability: part II. *J. Atmos. Sci.* 27:721–27

Sverdrup HU. 1953. On conditions for the vernal bloom of phytoplankton. *J. Cons. Int. Explor. Mer* 18:287–95

Tandon A, Garrett C. 1994. Mixed layer restratification due to a horizontal density gradient. *J. Phys. Oceanogr.* 24:1419–24

Taniguchi DAA, Franks PJS, Poulin FJ. 2014. Planktonic biomass size spectra: an emergent property of size-dependent physiological rates, food web dynamics, and nutrient regimes. *Mar. Ecol. Prog. Ser.* 514:13–33

Taylor J, Ferrari R. 2009. On the equilibration of a symmetrically unstable front via a secondary shear instability. *J. Fluid Mech.* 622:103–13

Taylor J, Ferrari R. 2011a. Ocean fronts trigger high latitude phytoplankton blooms. *Geophys. Res. Lett.* 38:L23601

Taylor J, Ferrari R. 2011b. Shutdown of turbulent convection as a new criterion for the onset of spring phytoplankton blooms. *Limnol. Oceanogr.* 56:2293–307

Thomas LN. 2005. Destruction of potential vorticity by winds. *J. Phys. Oceanogr.* 35:2457–66

Thomas LN, Lee CM. 2005. Intensification of ocean fronts by down-front winds. *J. Phys. Oceanogr.* 35:1086–102

Thomas LN, Rhines PB. 2002. Nonlinear stratified spin-up. *J. Fluid Mech.* 473:211–44

Thomas LN, Tandon A, Mahadevan A. 2008. Submesoscale processes and dynamics. In *Ocean Modeling in an Eddying Regime*, ed. MW Hecht, H Hasumi, pp. 17–38. Geophys. Monogr. Vol. 177. Washington, DC: Am. Geophys. Union

Tintore J, Gomis D, Alonso S, Parrilla G. 1991. Mesoscale dynamics and vertical motion in the Alboran Sea. *J. Phys. Oceanogr.* 21:811–23

Williams RG, Follows MJ. 1998. The Ekman transfer of nutrients and maintenance of new production over the North Atlantic. *Deep-Sea Res. I* 45:461–89

Annual Review of Marine Science

Volume 8, 2016

Contents

Errata

An online log of corrections to *Annual Review of Marine Science* articles may be found at http://www.annualreviews.org/errata/marine